12th March 2014

Hydrothermal Conversion of One-Photon-Fluorescent Poly-(4-vinylpyridine) into Two-Photon-Fluorescent Carbon Nanodots

Katherine Lawrence[a], Fengjie Xia[a,b], Rory L. Arrowsmith[a], Haobo Ge[a], Geoffrey W. Nelson[c], John S. Foord[c], Mónica Felipe-Sotelo[d], Nick D.M. Evans[d], John M. Mitchels[a], Stephen E. Flower[a], Stanley W. Botchway[e], Daniel Wolverson [f], Gazi N. Aliev [f], Tony D. James[a], Sofia I. Pascu[a]* and Frank Marken[a]*

[a] Department of Chemistry, University of Bath, Claverton Down, Bath BA2 7AY, UK

[b] State Key Laboratory of Advanced Technology for Materials Synthesis and Processing, Wuhan University of Technology, 430070, China

[c] Chemistry Research Laboratories, Oxford University, South Parks Road, Oxford OX1 3TA, UK

[d] Department of Chemistry, Loughborough University, Loughborough, Leicestershire, LE11 3TU, UK

[e] Central Laser Facility, Rutherford Appleton Laboratory, Research Complex at Harwell, STFC Didcot OX11 0QX, UK

[f] Department of Physics, University of Bath, Claverton Down, Bath BA2 7AY, UK

To be submitted to Langmuir

ABSTRACT: A novel two-photon-fluorescent N,O-heteroatom-rich carbon nanomaterial has been synthesized and characterized. The new carbon nanoparticles were produced by hydrothermal conversion from a one-photon-fluorescent poly-(4-vinylpyridine) precursor (P4VP). The carbonized particles (cP4VP-dots) with non-uniform particle diameter (ranging from sub-6 nm to 20 nm with some aggregates up to 200 nm) exhibit strong fluorescent properties in different solvents and have also been investigated for applications in cell culture media. The cP4VP-dots retain their intrinsic fluorescence in a cellular environment and exhibit an average excited state lifetime of 2.0 ± 0.9 ns in cell. The cP4VP-dots enter HeLa cells and do not cause significant damage to outer cell membranes. They provide one-photon or two-photon fluorescent synthetic scaffolds for imaging applications and/or drug delivery.

INTRODUCTION

Carbon nanodots (or c-dots) are a family of carbon-based nanomaterials (compare q-dots[1,2]) first proposed and isolated in 2004 by Xu et al. when purifying single wall carbon nanotubes (SWCNTs) prepared via arc-discharge methods.[3] C-dots are nanocarbons comprising discrete nanoparticles with diameters in the region of 10 nm that exhibit intrinsic fluorescent properties.[4,5] Shaowei Chen and coworkers demonstrated that soot-like materials when treated under hydrothermal conditions exhibit photo-luminescence due to alteration of surface functional groups.[6] A number of approaches for the synthesis of such materials have been developed and reported.[6,7] These methods include top-down methods, such as arc-discharge[3], electrochemical[8-11] and laser ablation methods[12-14] (which involve breaking down large carbonaceous materials into nano-sized carbon), or bottom-up methods (which involve the formation of c-dots from molecular precursors) based on synthetic supports[4,15], microwave methods[16], combustion[17,18] or hydrothermal techniques.[4,5,19] C-dots possess intrinsic luminescent properties which makes them excellent alternatives to quantum dots (QDs).[20] QDs are metal-based fluorescent semiconductor nanomaterials most commonly used for bioimaging, sensing and photovoltaic applications; however, they are often inherently toxic towards live cells.[11,21] Due to the environmental and biological hazards of QDs, c-dots may provide excellent less hazardous low cost replacements.[22]

Herein, we report a simple hydrothermal method for the formation of a hetero-carbon nanomaterial, fluorescent cP4VP-dots from a one-photon-fluorescent poly-(4-vinylpyridine) precursor. The amorphous cP4VP-dots show strong one- and two-photon-fluorescent properties that are weakly pH and solvent dependent. The potential of cP4VP-dots to be used in bioimaging applications is explored. The cP4VP-dots show apparent biocompatibility as evidenced by confocal fluorescence imaging and fluorescence lifetime imaging (FLIM) techniques. Furthermore the combined technique of FLIM and two- or multi-photon excitation in live biological imaging provides further advantages such as reduced cellular toxicity and deep tissue penetration. The excited state fluorescence lifetime of these nanoparticles was estimated in cellular media (EMEM, Eagle's Modified Essential Medium) and compared to the corresponding lifetime in organic (DMSO) solvent. Measurements indicate that the properties of nanoparticles are not affected by the change in their chemical environment. Even without surface functionalization, the most highly dispersed cP4VP-dots show intrinsic fluorescence and are visualized by confocal fluorescence microcopy to bind to the exterior of the cells without causing apparent damage to the outer cell membrane within the time-scale of cellular imaging experiments, of 1 h.

EXPERIMENTAL

Reagents

All reagents were used as supplied, without further purification: poly-(4-vinylpyridine), typical Mw 60,000 (Aldrich), acetic acid (Aldrich, 99.7 %, ACS reagent), absolute ethanol (Sigma-Aldrich), dimethyl sulfoxide (Sigma-Aldrich, >99.5 %), ortho-phosphoric acid (Fisher Scientific), sodium hydroxide (Aldrich, Sigma ultra, 98%). Demineralized and filtered water was taken from a Thermo Scientific water purification system (Barnstead Nanopure) with not less than 18.2 MΩ resistivity.

Instrumentation

X-ray photoelectron spectroscopy (XPS) was conducted using an Al Kα X-ray anode with energy of 1486.6 eV. All peaks were calibrated to the adventitious C1s peak (i.e. to 285 eV). Peaks were curve-fitted using the XPSPeak program version 4.1. Zeta potential and particle size measurements were obtained using a ZetaMaster S (Malvern Instruments Ltd, UK). Particle size measurements were validated with NIST traceable nanobeads™, a polystyrene polymer size standard (220 ± 6 nm, Polysciences Inc., Warrington, UK). To verify zeta potential measurements, zeta potential transfer standard (-50 mV ± 5, Malvern Instruments Ltd, UK) was used. The data was recorded using ZetaMaster S standard software PCS v1.41. UV/Vis spectra were obtained on Lambda 20 UV/Vis spectrometer (PerkinElmer, USA) with UV winlab version 2.70.01 software. Fluorescence measurements were recorded on fluoroSENS fluorimeter (Gilden Photonics, UK) with fluoroSENS system software version 1.88.7 and LS50b luminescence spectrometer (Perkin Elmer, USA) with FL winlab version 4.00.02 software. Fourier transform infrared (FTIR) spectra were recorded on a Spectrum 100 FTIR-Spectrometer (PerkinElmer, USA) and Spectrum Express software. A JEM1200EXII (JEOL, Japan) transmission electron microscope (TEM) was used for imaging the P4VP starting material and cP4VP-dots (80 kV with 0.025 pA cm^{-2} probe 8 on Cu grids 1000 mesh with 2 nm amorphous carbon film pH 8 hyrophylised and deposited from ethanol).

For bio-imaging studies, a multi-photon excitation technique was used. Laser light with wavelength of 810 nm (for single photon fluorescence at excitation wavelength 488 nm was used see supporting information) was obtained from an optical parametric oscillator pumped by a pulsed mode locked titanium sapphire laser (Mira F900, Coherent Inc. Lasers, US)

that produced 180 femtosecond pulses at 75 MHz. This in turn was pumped by a solid-state continuous wave 532 nm laser (Verdi V8, Coherent Inc. Lasers, US). The oscillator's fundamental output of 810 ± 2 nm was also used for the multi-photon excitation. The laser beam was focused to a diffraction-limited spot through a high numerical aperture (1.2) microscope objective, Nikon Corporation, Japan). Samples were illuminated at the stage of an inverted microscope (Nikon TE2000-U). An X-Y galvanometer (CGS Lumonics, US) was used to raster scan the focused laser spot for imaging. Fluorescence emission data was generated without descanning, bypassing the scanning system and passing through a BG39 colored glass optical filter, the signals were detected with an external fast microchannel plate photomultiplier tube (R3809-U, Hamamatsu, Japan). The components were linked via a Time-Correlated Single Photon Counting (TCSPC) module (SPC830, Becker & Hickl GmbH, Berlin).

cP4VP-dots were dispersed in 1: 99 DMSO: EMEM and fluorescence lifetime measurements were recorded using a TCSPC (Becker & Hickl GmbH, Berlin) following excitation wavelength of 810 ± 2 nm, with emissions at 360-580 nm.. Two photon induced emission spectra data was obtained with an Acton Research Component 275 Spectrograph (Princeton Instruments, US) and an Andor iDus 420-BU CCD camera (Andor Technology, Belfast). Lifetime calculations were carried out using Becker & Hickl SPCImage Analysis software.

For MTT assays[23] cells were seeded as 7 x 10^4 cells mL^{-1} and allowed to adhere for 2 days. Subsequently cPV4P-dots were added with final concentrations of 500 µg/mL, 100 µg/mL, 50 µg/mL, 10 µg/mL, 1 µg/mL, 0.1 µg/mL, 10 ng/mL and 1 ng/mL, each with 1% DMSO and incubated for 2 days at 37°C. Cells were 3 times washed with 100 µL PBS and incubated with 100 µL of 0.5 mg/mL MTT (1:9, PBS: serum free medium) for 3 hours. The media was aspirated, 100 µL DMSO was added and the absorbance was read at 570 nm (with a FLUOstar Omega system).

Hydrothermal Synthesis

400 mg of P4VP was dissolved by sonication in 20 mL of 1 mM acetic acid for 30 minutes. The solution was transferred into a 125 mL high pressure vessel (Parr Instrument Company) and heated at 200°C for 12 h. After cooling down, a dark solid was removed by filtration and copiously washed with water. The solid was dissolved in ethanol and dried in vacuo to give a shiny brown solid (see photograph in Figure 1a, 47 % yield, elemental analysis $C_7H_{7.25}NO_{0.5}$) which was collected and characterized by XPS, TEM, zeta potential measurements, IR, UV/vis spectroscopy and fluorescence experiments.

RESULTS AND DISCUSSION

Figure 1b shows a typical TEM image of cP4VP-dots with broad size distribution (estimated as typically less than 6 nm but up to 30 nm, see Figure 1d, composed of C, N, O, see Figure 1c) with some larger aggregates with a diameter of up to ~200 nm. The photograph in Figure 1a demonstrates the colour change from white to dark brown after hydrothermal carbonization (see scheme in Figure 1e) indicative of a broader absorption reaching into the infrared.

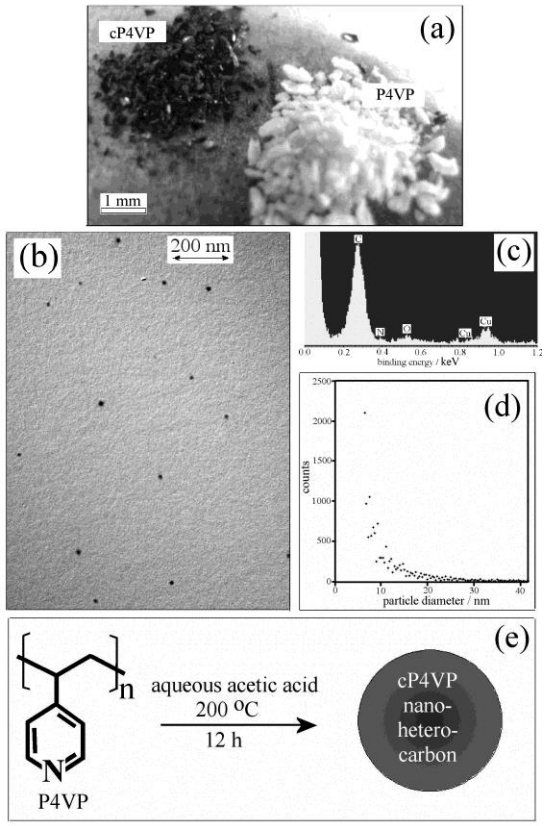

Figure 1. (a) Photograph of white P4VP precursor material and black-brown cP4VP-dot product. (b) TEM image of cP4VP-dots. (c) EDX analysis and (d) particle size analysis with 6 nm instrumentation cut-off. (e) Reaction scheme for hydrothermal conversion.

The starting P4VP polymer and the carbonized cP4VP-dots were investigated using XPS (see Figure 2). The P4VP starting material showed a single N1s peak with a binding energy of 398.8 eV, this is consistent with the sp^2 hybridized nitrogen in the pyridine rings. The C1s signal was deconvoluted into two peaks associated with C-C/C-H carbon (285.0 eV) and C-N from the pyridine functionality (286.0 eV). In addition to this, a C1s "shake-up" peak was observed at 292.0 eV. This signal is consistent with photoelectrons interacting with π-π* transitions associated with the aromatic pyridine ring systems.[24] There is also a signal of weak intensity corresponding to O1s at binding energy 531.8 eV and this is thought to be due to slow oxidation of the polymer surface due to ageing.

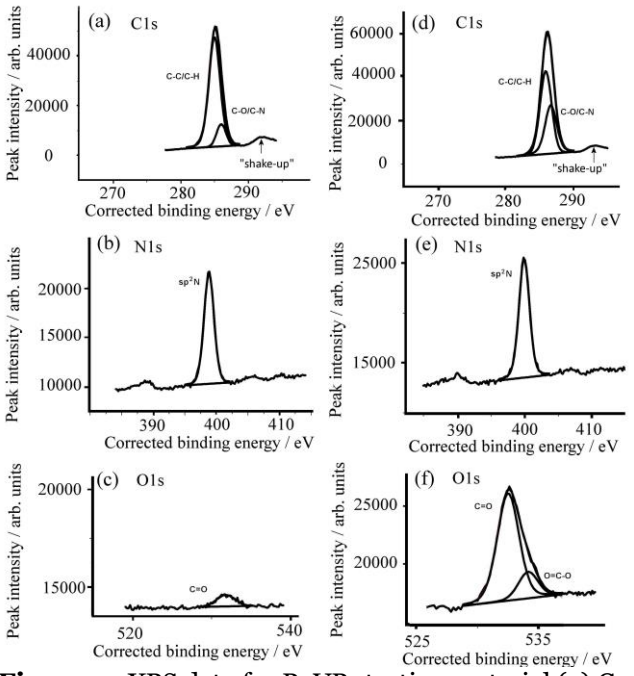

Figure 2. XPS data for P4VP starting material (a) C1s (b) N1s (c) O1s and cP4VP-dots (d) C1s (e) N1s (f) O1s.

In comparison to the starting material XPS data, the carbonized cP4VP-dots show many similarities. The intensity of the N1s signal has a high N1s/C1s ratio (0.10) indicating that this sample has a photoelectron signal intensity close to that of the P4VP polymeric starting material. Also, the N1s peak at 398.2 eV and C1s and C1s "shake up" peaks are of similar binding energies to that observed for the P4VP starting material. The main difference between the two samples can be seen when examining the O1s signals. In contrast to the starting material, the carbonized cP4VP-dots showed a strong signal that could be resolved into two peaks of binding energies 531.6 and 533.3 eV, which are due to carbonyl and carboxyl oxygen, respectively.[25] This is thought to be due to oxidation/hydrolysis processes that occur during the hydrothermal carbonization of the material. From the XPS analysis, it is clear that in the synthesized material much of the starting material functionality is maintained. New oxygen functionalities indicate that carbonyl and carboxylate groups decorate the cP4VP-dot surface.

Figure 3 shows the FT-IR spectrum of these cP4VP-dots. A broad peak is seen at 3300 cm^{-1} ascribed (in comparison to the P4VP starting material) to an N-H stretch of the protonated pyridinium ring. The adsorption bands at 3030 and 2920 cm^{-1} are characteristic of the aromatic C-H stretching vibrations of the CH_2 groups in the pyridine ring and the asymmetric vibrations of the CH_2 groups, respectively. A peak is observed at 1650 cm^{-1} due to the N-H bending. A small C=O peak can be observed at ~1700 cm^{-1} which is absent from the starting material. This is only a small peak as it is likely that only some of the outer surface has become oxidized during hydrothermal conversion The core material will resemble P4VP starting material, as confirmed by elemental analysis (P4VP: C_7H_7N and cP4VP-dots: $C_7H_{7.25}NO_{0.5}$). Most importantly, there is a sharp, strong band observed at 1600 cm^{-1} which shows the stretching vibrations of the pyridine ring. This demonstrates that the pyridine functionality has been at least in part retained during the carbonization process. Adsorption bands between 1220 and 880 cm^{-1} can be attributed to the amine C-N stretch and the peak at 820 cm^{-1} is indicative of pyridine ring out-of-plane bending.

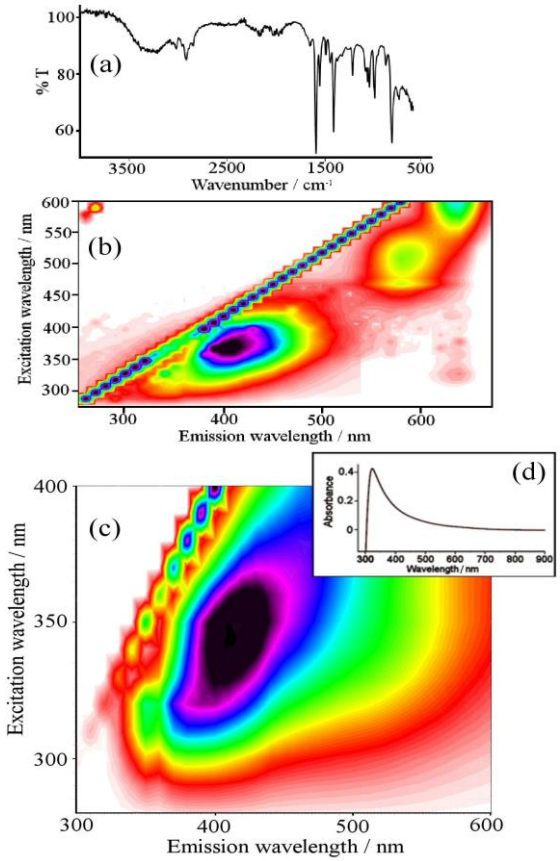

Figure 3. (a) Solid state FTIR spectrum for cP4VP-dots. (b) 3D fluorescence mapping of the P4VP polymeric starting material dissolved in EtOH (1 mg mL^{-1}). Fluorescence mapping (c) and UV/Vis spectrum (d) for cP4VP-dots in DMSO (1 mg mL^{-1}) showing that the maximum emission (at 410 nm) is observed when the excitation wavelength is 350 nm in agreement with the maximum UV/Vis absorbance.

The zeta potential was measured for the cP4VP-dots as a function of pH. A solution of cP4VP-dots was prepared in DMSO and then diluted to a concentration of 1 μg mL^{-1} with 0.1 M phosphate buffer at different pH values at a ratio of 50:50 DMSO: buffer. The zeta potential across a pH range from 2 to 12 was

relatively constant at approximately -7 ± 2 mV. This value suggests a weak charge perhaps linked to carboxylates.[26] Zeta potential measurements indicate that the isoelectric point of the cP4VP-dots occurs at approximately pH 2. However, over the entire pH range, the cP4VP-dots in DMSO:buffer are relatively unstable and form aggregates, presumably due to the low zeta potential. UV/Vis measurements of 1 mg mL^{-1} cP4VP-dots in DMSO showed a peak at 350 nm (Figure 3d). This correlated well with a 3-dimensional map of excitation wavelength versus emission wavelength for the same sample (Figure 3c). The 3-D contour map clearly shows that the greatest emission is seen at 410 nm with an excitation wavelength of 350 nm. In comparison, 3D fluorescence mapping for the P4VP polymeric starting material dissolved in EtOH shows the main fluorescence response at an excitation of 370 nm with corresponding emissions at 390 and 410 nm. Further emissions were observed at 580 nm for excitations at 470 and 510 nm, and 630 nm for excitation at 600 nm. The relative quantum yield for the cP4VP-dots was determined by comparison to a $[Ru(bipy)_3](PF_6)_2$ standard in water with a known quantum yield of 4.2% following equation (1), where Φ = relative quantum yield, D = integrated area of fluorescence emission peak, A = absorbance at the excitation wavelength, I = flux at the excitation wavelength and η = refractive index (subscript R and S refer to the reference and the sample, respectively).

$$\Phi_S = \Phi_R \times \left(\frac{D_S}{D_R}\right) \times \left(\frac{A_R}{A_S}\right) \times \left(\frac{I_R}{I_S}\right) \times \left(\frac{\eta_S}{\eta_R}\right)^2 \qquad (1)$$

The cP4VP-dots show a quantum yield of ~3 % at an excitation wavelength of 350 nm. The quantum yield of the majority of cP4VP-dots is below 1 % and not to the magnitude of QDs, however, this simple and effective method which requires minimal work up, results in improved quantum yield without the need for surface passivation.[9, 17, 27]

The effect of solvent on the fluorescence emission was investigated as shown in Figure 4. By comparing DMSO, a polar aprotic solvent, with ethanol and chloroform, polar protic and non-polar respectively, a clear shift in the maximum fluorescence intensity was observed. This bathochromic shift is due to stabilization of the excited state fluorophore in more polar solvents, i.e. in DMSO. A shift of 11 nm (0.084 eV) is observed when changing from chloroform to ethanol and a shift of 20 nm (0.15 eV) from chloroform to DMSO.

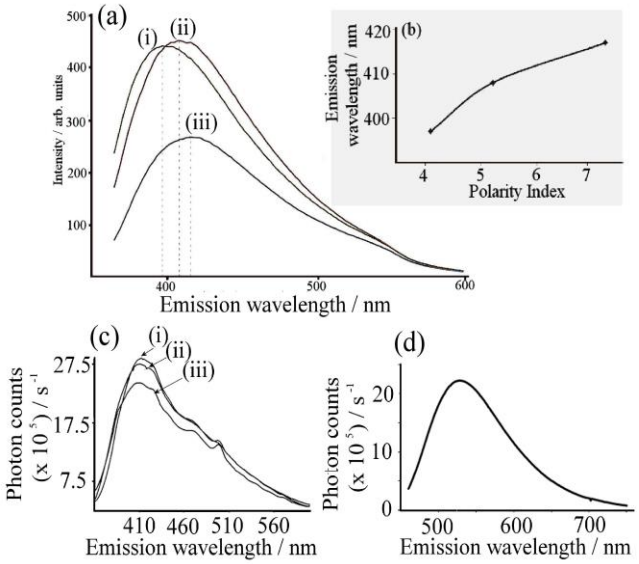

Figure 4. (a) Fluorescence emission spectra at an excitation wavelength of 350 nm for 1 mg mL^{-1} cP4VP in (i) chloroform (ii) ethanol and (iii) DMSO (b) A plot of the emission wavelength for the maximum fluorescence intensity versus the polarity index of the solvent.[28] (c,d) Single photon fluorescence emission spectra at excitation wavelength (c) 350 nm in 50 : 50 DMSO : 0.1 M phosphate buffer solution (i) pH 2 (ii) pH 7 (iii) pH 12 and (d) at excitation wavelength 455 nm in DMSO.

The pH effect on the fluorescence was investigated and only minor changes in maximum wavelength were observed (see Figure 4c). A slight decrease in intensity of the signal was likely to be caused by the colloidal aggregation. The maximum of the emission shifted by 5 nm between pH 2 and pH 7 and a further 5 nm when the pH was adjusted from 7 to pH 12, averaging 1 nm per pH unit. In summary, there appears to be little effect of pH (e.g. no pyridine/pyridinium equilibrium) possibly due to the chromophore being buried within the particle core.

Two-photon time correlated single-photon counting (TCSPC) fluorescence lifetime and emission data of cP4VP-dots are given in Figure 5b and 5f, respectively. The observed short lived component of a three component lifetime may be due to aggregation of the sample (ps order lifetime). A good fit, with a χ^2 value of 1.13, was obtained for three exponential components analysis of the decay data, Figure 5b. The three-component exponential fit gave a pre-exponential factor of 37.9% with a lifetime of 0.1 ns 41.4% with a lifetime of 1.5 ns and 20.7% with a lifetime of 5.8 ns (λ_{ex} = 810 nm, a two photon excitation process). In contrast, P4VP exhibited negligible fluorescence when exposed to two-photon excitation. The single-photon TCSPC data trace with excitation at 405 nm, however, resulted in a single component lifetime of 2.1 ns, data with a

fitting parameter of $\chi^2 = 1.35$. These excited state lifetime difference between the cP4VP-dots and P4VP further indicates a molecular electronic state difference that may be contributing to the two-photon emission nature of the former. As yet these electronic states are unknown.

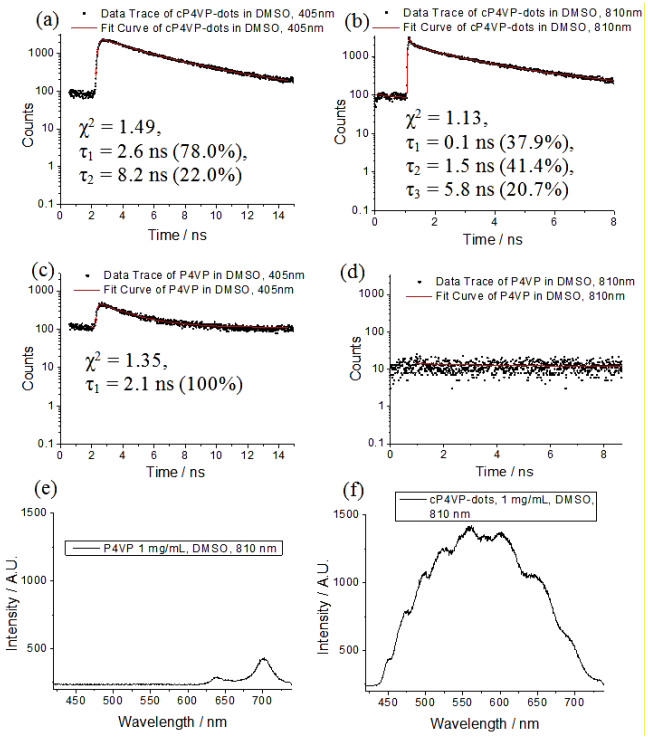

Figure 5. TCSPC decay curves in DMSO (1 mg mL^{-1}) for (a) single-photon excitation with 405 nm of cP4VP-dots, (b) two-photon excitation with 810 nm of cP4VP-dots, (c) single-photon excitation with 405 nm of P4VP, (d) two-photon excitation with 810 nm of P4VP. Emission spectra (1 mg mL^{-1}) with 810 nm excitation of (e) P4VP and (f) cP4VP-dots.

High-resolution confocal imaging under single-photon (405, 488 and 543 nm) or two-photon excitation (810 nm), using a mode-locked Ti-sapphire laser, was employed to generate images of the dispersed cP4VP-dots in cellular media by the raster scanning of the laser spot in the xy plane. Figure 6 shows single-photon scanning confocal microscopy images for cP4VP-dots incubated in HeLa cells.

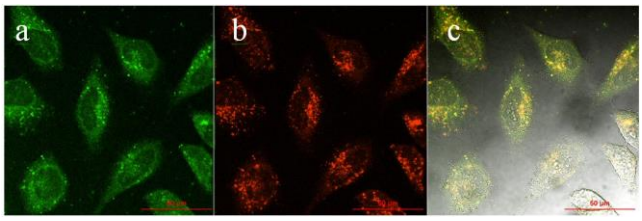

Figure 6. Single-photon laser scanning confocal imaging of cP4VP-dots colocalized with lysotracker red® (200 nM) in HeLa cells incubated at 37°C for 1 h in 1: 99 DMSO: EMEM. Micrograph (a) represents excitation with 488 nm (long pass 515 nm), (b) excitation with 543 nm (long pass 606 nm and (c) an overlay of (a), (b) and the DIC channel.

Confocal fluorescence imaging, coupled with fluorescence lifetime imaging microscopy (FLIM) following multi-photon excitation with near infrared (NIR) femtosecond laser pulses are widely used in the study of small molecule fluorophores particularly for in vitro imaging studies.[29-31] To date, FLIM has been used primarily on common fluorescent dyes (e.g. GFP-tagged proteins, fluorescein-based derivatives as well as indole containing compounds).[32,33] Recent work explored lifetime imaging of fluorescent carbon nanotube complexes which permitted, for the first time, to probe functional carbon nanomaterials' integrity in a cellular environment.[34] The combination of two-photon excitation with FLIM allows the use of NIR light to provide deeper tissue penetration, reduced cellular cytotoxicity and scattering. Exploiting the sensitivity of lifetime measurements which is independent of intensity, excited state lifetime measurements were used to provide a method for studying the integrity of the newly synthesized cP4VP-dots in cellular media.

Two photon fluorescence imaging and emission lifetime measurements were carried out, for HeLa cell lines loaded with the cP4VP-dots (Figures 6 and 7). Single-photon laser scanning confocal fluorescence imaging showed the nanoparticles retained fluorescence emission under single photon excitation (λ_{ex} 405 and 488 nm) in the presence of cells. The controls show weak fluorescence intensity assignable to cell auto-fluorescence when excited at 405 nm. At this wavelength the fluorescence from the cP4VP-dot was just above the auto-fluorescence background. However the 488 nm excitation shows clearly higher signal intensity with respect to background auto-fluorescence.

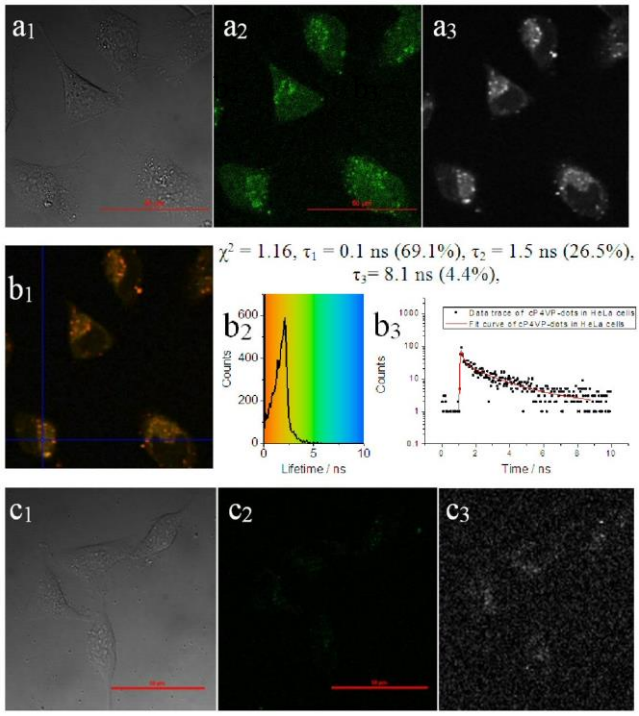

Figure 7. Fluorescence microscopy of at 10 μg/mL cP4VP-dots (a and b) and P_4VP (c). Single-photon laser scanning confocal imaging of HeLa cells incubated at 37°C for 1 h in 1: 99 DMSO: EMEM for ($a_{1\text{-}2}$ and $c_{1\text{-}2}$), λ_{ex} = 488 nm (scale bar 50 μm), green channel (long pass filtered at 515 nm) (a_2, c_2). Two-photon confocal fluorescence (λ_{ex} = 810 nm) intensity image (a_3, c_3), τ_m lifetime mapping (b_1), corresponding lifetime distribution curve in ns (b_2) and sample point decay trace (b_3) displaying significantly stronger emission when incubated with cP4VP-dots than with P4VP. Lack of emission resulting from two-photon excitation of P4VP incubated in cells (Figure 7 c_3) meant that data fitting could not be achieved.

The localization in organelles and cellular uptake mechanism were investigated using laser scanning confocal microscopy. cP4VP-dots and lysotracker red® *(Invitrogen)* were incubated for 1h in HeLa (Figure 6), which demonstrated strong colocalization, indicating that the polymer localizes within the lysosome (probably in part due to the hydrophobic nature of cP4VP). Moreover, uptake at 4°C was very weak *(ESI)*, signifying that the uptake mechanism was *via* active processes, with negligible uptake *via* passive diffusion. Furthermore, the non-carbonized P4VP precursor material did not enter cells and displayed insignificant fluorescence *via* laser scanning confocal microscopy (Figure 7). To further probe the potential of cP4VP-dots as traceable imaging probes inside living cells, two-photon emission decay lifetime spectroscopy was applied. First, the emission spectra were recorded following pulsed laser excitation (λ_{ex} = 810 nm in DMSO). DMSO was selected as the solvent of choice as the cP4VP-dots showed minimum scattering minimizing aggregation within the experimental timescale in this solvent and due to its low volatility. Secondly, excited state lifetimes were recorded by time-correlated single-photon counting with a less than 40 ps instrument response function. To verify that the new materials remain stable *in vitro* with respect to decomposition, fluorescence emission lifetime measurements were carried out using two-photon FLIM in presence of HeLa cell lines (1 h incubation, 37 °C, using 810 nm). In both systems (solution experiments in DMSO *versus in vitro* imaging in the presence of HeLa cells), these nanoparticles exhibited strong fluorescence emission with more than one lifetime component: calculations (SPC Image analysis software) indicated a long component on the order of several nanoseconds of ca. 8 ns in HeLa cells for highly dispersed particles, a shorter component of ca. 1.5 to 2.5 ns and a much shorter component of ca. 0.15 ns for aggregated cP4VP-dots. The highly-dispersed cP4VP-dots have an average mean lifetime (τ_m) of 2.0 ns ± 0.9 ns FWHH (Figure 7). To investigate the cytotoxicity of the cP4VP-dots MTT assays were carried out. The MI_{50}, the concentration required to reduce the metabolic function of mitochondria to 50% was determined to be 64 μg/mL ± 8 μg/mL over six experiments. This concentration was significantly greater than which was used to visualize cells (10 μg/mL), in agreement with the minimal effect observed on cell morphology (see Figure ESI19).

CONCLUSION

In summary, we have exploited a simple hydrothermal conversion synthesis for the formation of a novel two-photon fluorescent hetero-carbon nanomaterial from a one-photon fluorescent precursor. cP4VP-dots have been characterized using XPS, IR, zeta potential measurements and TEM. The amorphous cP4VP-dots exhibited strong fluorescent properties that show only insignificant pH but significant solvent dependency in single photon fluorescence experiments. The hydrothermal conversion is demonstrated to "switch on" a two-photon fluorescent mode whilst maintaining strong single-photon fluorescence. Finally, the potential for bioimaging applications was investigated. The cP4VP-dots retained their intrinsic fluorescence in cell medium and the most highly dispersed particles were seen to enter HeLa cells apparently without causing significant damage to the outer cell membrane. This approach could provide an excellent new and general pathway for developing non-toxic nanomedicines and novel synthetic scaffolds for future applications as traceable imaging probes inside living cells.

ASSOCIATED CONTENT

Supporting Information. Fluorescence mapping at different pH values, control confocal images of HeLa cells, im-

ages and fluorescence lifetimes of nanoparticles after 15 minutes and 1 hour in different parts of the cell culture medium. This material is available free of charge via the Internet at http://pubs.acs.org

AUTHOR INFORMATION

Corresponding Authors:

* s.pascu@bath.ac.uk and * f.marken@bath.ac.uk

ACKNOWLEDGMENT

K.L. thanks the EPSRC for a DTA studentship to fund this research. This work was also supported by the CSC (China Scholarship Council, file number 2010695033) for F.X. S.I.P and S.W.B. thank the Royal Society, STFC and MRC for funding towards the imaging work.

REFERENCES

1. Alivisatos, A.P.; Gu, W.W.; Larabell, C., Quantum dots as cellular probes. Ann. Rev. Biomed. Engineer. 2005, 7, 55-76.
2. Baker, S. N.; Baker, G. A., Luminescent Carbon Nanodots: Emergent Nanolights. Angewandte Chemie-International Edition 2010, 49 (38), 6726-6744.
3. Xu, X. Y.; Ray, R.; Gu, Y. L.; Ploehn, H. J.; Gearheart, L.; Raker, K.; Scrivens, W. A., Electrophoretic analysis and purification of fluorescent single-walled carbon nanotube fragments. J. Am. Chem. Soc. 2004, 126 (40), 12736-12737.
4. Bourlinos, A. B.; Stassinopoulos, A.; Anglos, D.; Zboril, R.; Georgakilas, V.; Giannelis, E. P., Photoluminescent carbogenic dots. Chem. Mater. 2008, 20 (14), 4539–4541.
5. Lu, W.; Qin, X.; Liu, S.; Chang, G.; Zhang, Y.; Luo, Y.; Asiri, A. M.; Al-Youbi, A. O.; Sun, X., Economical, Green Synthesis of Fluorescent Carbon Nanoparticles and Their Use as Probes for Sensitive and Selective Detection of Mercury(II) Ions. Anal. Chem. 2012, 84 (12), 5351–5357.
6. Tian, L.; Song, Y.; Chang, X.; Chen, S.W., Hydrothermally enhanced photoluminescence of carbon nanoparticles. Scripta Materialia 2010, 62, 883–886.
7. Titirici, M.-M.; Antonietti, M., Chemistry and materials options of sustainable carbon materials made by hydrothermal carbonization. Chem. Soc. Rev. 2010, 39 (1), 103-116.
8. Zheng, L.; Chi, Y.; Dong, Y.; Lin, J.; Wang, B., Electrochemiluminescence of Water-Soluble Carbon Nanocrystals Released Electrochemically from Graphite. J. Am. Chem. Soc. 2009, 131 (13), 4564–4565.
9. Zhao, Q.-L.; Zhang, Z.-L.; Huang, B.-H.; Peng, J.; Zhang, M.; Pang, D.-W., Facile preparation of low cytotoxicity fluorescent carbon nanocrystals by electrooxidation of graphite. Chem. Commun. 2008, (41), 5116-5118.
10. Zhou, J.; Booker, C.; Li, R.; Zhou, X.; Sham, T.-K.; Sun, X.; Ding, Z., An electrochemical avenue to blue luminescent nanocrystals from multiwalled carbon nanotubes (MWCNTs). J. Am. Chem. Soc. 2007, 129 (4), 744-745.
11. Ming, H.; Ma, Z.; Liu, Y.; Pan, K.; Yu, H.; Wang, F.; Kang, Z., Large scale electrochemical synthesis of high quality carbon nanodots and their photocatalytic property. Dalton transactions (Cambridge, England : 2003) 2012, 41 (31), 9526-9531.
12. Cao, L.; Wang, X.; Meziani, M. J.; Lu, F.; Wang, H.; Luo, P. G.; Lin, Y.; Harruff, B. A.; Veca, L. M.; Murray, D.; Xie, S.-Y.; Sun, Y.-P., Carbon dots for multiphoton bioimaging. J. Am. Chem. Soc. 2007, 129 (37), 11318–11319.
13. Hu, S.-L.; Niu, K.-Y.; Sun, J.; Yang, J.; Zhao, N.-Q.; Du, X.-W., One-step synthesis of fluorescent carbon nanoparticles by laser irradiation. J. Mater. Chem. 2009, 19 (4), 2367–2375.
14. Sun, Y. P.; Zhou, B.; Lin, Y.; Wang, W.; Fernando, K. A. S.; Pathak, P.; Meziani, M. J.; Harruff, B. A.; Wang, X.; Wang, H. F.; Luo, P. J. G.; Yang, H.; Kose, M. E.; Chen, B. L.; Veca, L. M.; Xie, S. Y., Quantum-sized carbon dots for bright and colorful photoluminescence. J. Am. Chem. Soc. 2006, 128 (24), 7756–7757.
15. Liu, R.; Wu, D.; Liu, S.; Koynov, K.; Knoll, W.; Li, Q., An Aqueous Route to Multicolor Photoluminescent Carbon Dots Using Silica Spheres as Carriers. Angewandte Chemie-International Edition 2009, 48 (25), 4598-4601.
16. Zhu, H.; Wang, X.; Li, Y.; Wang, Z.; Yang, F.; Yang, X., Microwave synthesis of fluorescent carbon nanoparticles with electrochemiluminescence properties. Chem. Commun. 2009, (34), 5118-5120.
17. Ray, S. C.; Saha, A.; Jana, N. R.; Sarkar, R., Fluorescent Carbon Nanoparticles: Synthesis, Characterization, and Bioimaging Application. J. Phys. Chem. C 2009, 113 (43), 18546–18551.
18. Tian, L.; Ghosh, D.; Chen, W.; Pradhan, S.; Chang, X.; Chen, S., Nanosized Carbon Particles From Natural Gas Soot. Chem. Mater. 2009, 21 (13), 2803-2809.
19. Hsu, P.-C.; Chang, H.-T., Synthesis of high-quality carbon nanodots from hydrophilic compounds: role of functional groups. Chem. Commun. 2012, 48 (33), 3984-3986.
20. Yang, Y.; Cui, J.; Zheng, M.; Hu, C.; Tan, S.; Xiao, Y.; Yang, Q.; Liu, Y., One-step synthesis of amino-functionalized fluorescent carbon nanoparticles by hydrothermal carbonization of chitosan. Chem. Commun. 2012, 48 (3), 380-382.
21. Li, H.; He, X.; Kang, Z.; Huang, H.; Liu, Y.; Liu, J.; Lian, S.; Tsang, C. H. A.; Yang, X.; Lee, S.-T., Water-Soluble Fluorescent Carbon Quantum Dots and Photocatalyst Design. Angewandte Chemie-International Edition 2010, 49 (26), 4430-4434.
22. Yang, S.-T.; Wang, X.; Wang, H.; Lu, F.; Luo, P. G.; Cao, L.; Meziani, M. J.; Liu, J.-H.; Liu, Y.; Chen, M.;

Huang, Y.; Sun, Y.-P., Carbon Dots as Nontoxic and High-Performance Fluorescence Imaging Agents. J. Phys. Chem. C 2009, 113 (42), 18110-18114.

23. Arrowsmith, R.L.; Waghorn, P.A.; Jones, M.W.; Bauman, A.; Brayshaw, S.K.; Hu, Z.Y.; Kociok-Kohn, G.; Mindt, T.L.; Tyrrell, R.M.; Botchway, S.W.; Dilworth, J.R.; Pascu, S.I., Fluorescent gallium and indium bis(thiosemicarbazonates) and their radiolabelled analogues: Synthesis, structures and cellular confocal fluorescence imaging investigations Dalton Trans., 2011, 40 (23), 6238-6262.

24. Pels, J. R.; Kapteijn, F.; Moulijn, J. A.; Zhu, Q.; Thomas, K. M., Evolution of Nitrogen Functionalities in Carbonaceous Materials During Pyrolysis. Carbon 1995, 33 (11), 1641-1653.

25. Zhang, D.; Dougal, S. M.; Yeganeh, M. S., Effects of UV irradiation and plasma treatment on a polystyrene surface studied by IR-visible sum frequency generation spectroscopy. Langmuir 2000, 16 (10), 4528–4532.

26. Song, S.-H.; Lee, S. J.; Rhee, S.-H., Synthesis of biodegradable poly(epsilon-caprolactone)-organosiloxane hybrid with carboxylate groups. Journal of Biomedical Materials Research Part B-Applied Biomaterials 2012, 100B (5), 1289-1297.

27. Liu, H.; Ye, T.; Mao, C., Fluorescent carbon nanoparticles derived from candle soot. Angewandte Chemie-International Edition 2007, 46 (34), 6473-6475.

28. Fisher Scientific, http://www.fisher.co.uk/index.php/en/chemical-technical-tools/194-chemical-data--information-tables/1079-summary-of-key-physical-data-for-solvents. (accessed 24th September 2012).

29. Konig, K., Multiphoton microscopy in life sciences. J. Microsc. (Oxford) 2000, 200 (Copyright (C) 2011 American Chemical Society (ACS). All Rights Reserved.), 83-104.

30. Stutzmann, G. E.; Parker, I., Dynamic multiphoton imaging: a live view from cells to systems. Physiology 2005, 20, 15-21.

31. Oheim, M.; Michael, D. J.; Geisbauer, M.; Madsen, D.; Chow, R. H., Principles of two-photon excitation fluorescence microscopy and other nonlinear imaging approaches. Adv. Drug Delivery Rev. 2006, 58, 788-808.

32. Botchway, S. W.; Parker, A. W.; Bisby, R. H.; Crisostomo, A. G., Real-time cellular uptake of serotonin using fluorescence lifetime imaging with two-photon excitation. Microsc. Res. Tech. 2008, 71, 267-273.

33. Treanor, B.; Lanigan, P. M. P.; Suhling, K.; Schreiber, T.; Munro, I.; Neil, M. A. A.; Phillips, D.; Davis, D. M.; French, P. M. W., Imaging fluorescence lifetime heterogeneity applied to GFP-tagged MHC protein at an immunological synapse. J. Microsc. 2005, 217, 36-43.

34. Hu, Z.; Pantos, G. D.; Kuganathan, N.; Arrowsmith, R. L.; Jacobs, R. M. J.; Kociok-Koehn, G.; O'Byrne, J.; Jurkschat, K.; Burgos, P.; Tyrrell, R. M.; Botchway, S. W.; Sanders, J. K. M.; Pascu, S. I., Interactions Between Amino Acid-Tagged Naphthalenediimide and Single Walled Carbon Nanotubes for the Design and Construction of New Bioimaging Probes. Adv. Funct. Mater. 2012, 22 (3), 503-518.

Insert Table of Contents Artwork